



OPEN

Corrosion behavior of predominant *Halodesulfovibrio* in a marine SRB consortium and its mitigation using ZnO nanoparticles

Mansour Jafari¹, Hamid Moghimi¹✉, Hassan Tirandaz² & Mohammad-Bagher Ebrahim-Habibi²✉

Formation of Sulfate Reducing Bacteria (SRB) biofilm accelerates microbiologically influenced corrosion (MIC). The aim of this study was to investigate both the corrosivity of a marine SRB consortium on carbon steel coupons and its mitigation in the presence of ZnO. Metagenomics analysis revealed that *Halodesulfovibrio* (78.9%) was predominant and could be related to MIC. The analysis also showed a remarkable shift from a highly corrosive SRB consortium in the control bioreactors to a far less corrosive consortium when ZnO was added to the bioreactors. Further results indicated that the corrosion rate of the SRB consortium was 8.17 mpy on the carbon steel coupons. In the ZnO-treated bioreactors, the count of SRB and MIC in the carbon steel coupons simultaneously reduced. Moreover, Confocal Laser Scanning Microscopy and profilometry analysis determined that ZnO could significantly decrease the amount of biofilm and the corrosion rate. Electrochemical experiments revealed higher corrosion current density (i_{corr}) and lower charge transfer resistance (R_{ct}) in the control bioreactors relative to the ZnO-treated bioreactors. We introduce *Halodesulfovibrio* as a potentially important corrosive genus in a marine SRB consortium. Additionally, ZnO could be considered a proper candidate to control the corrosion induced by *Halodesulfovibrio*.

Keywords Consortium, *Halodesulfovibrio*, Microbial corrosion, ZnO

Development of Sulfate Reducing Bacteria (SRB) biofilms plays a crucial role in localized corrosion of metals, which is a serious concern in oil and gas industry operations¹. Biofilms are usually comprised of sessile cells, Extracellular Polymeric Substances (EPS), corrosion products and some organic and inorganic compounds obtained from the environment^{2,3}. It has been illustrated that biofilms which are mostly established in marine environments always encompass more than several species that cooperate to improve their survival chances⁴. Moreover, several studies demonstrate that consortium of SRB in an anaerobic marine condition accelerated the corrosion failures^{5,6}. Furthermore, studies indicate that salinity remarkably enhances the expression of genes associated with biofilm formation and sulfate reduction⁷. Therefore, it is obvious that microbiologically influenced corrosion (MIC) could be considerably induced in marine environment.

Desulfovibrio species are abundant in corrosion-affected equipment, including steel pipes and plates, located in the marine environment^{8,9}. Members of this genus have a metabolic versatility that enables them to reduce iron sulfate and, with hydrogen, generate H₂S^{9,10}. Furthermore, *Desulfotomaculum* species, which are gram-positive and thermophilic SRB, are of vital importance in MIC^{11,12}. Members of this genus have been isolated from crude oil field, oil production wells, or the cooling towers of a petroleum refinery^{11,12}. Recently, Vlasov et al. (2023) and coworkers have shown that *Halodesulfovibrio* species could contribute to MIC¹³. *Halodesulfovibrio* species are salt-loving *Desulfovibrio* that are strictly anaerobic and their metabolism is both respiratory and fermentative. In contrast, the metabolism of *Desulfovibrio* species is respiratory and it is sometimes fermentative. All species of the genus *Halodesulfovibrio* need high concentrations of NaCl to grow optimally. However, some *Desulfovibrio* species are moderately halophilic. The growth temperature for *Halodesulfovibrio* is 20–37 °C, while growth temperature for *Desulfovibrio* species is 25–35 °C^{14,15}. No experiments have been conducted to evaluate

¹Department of Microbiology, School of Biology, College of Science, University of Tehran, Tehran, Iran. ²Microbiology and Biotechnology Research Group, Research Institute of Petroleum Industry, Tehran, Iran. ✉email: hmoghimi@ut.ac.ir; habibi.mohamad@gmail.com

the corrosion behaviour of *Halodesulfovibrio* and more research is needed to understand its involvement in the promotion of corrosion processes.

In order to mitigate MIC, many investigations have been focused on formulating industrial biocides to tackle SRB biofilm formation^{16,17}. The Employment of biocides such as glutaraldehyde, isothiazolinone, Tetrakis Hydroxymethyl Phosphonium Sulfate (THPS) and quaternary ammonium compounds is typical in oilfields¹⁸. Studies indicate that these biocides are less effective when microorganisms are embedded into the biofilm matrix¹⁹. Additionally, SRB biocidal resistance has been reported in several studies in the presence of these biocides²⁰. Moreover, these compounds unfortunately cause significant damage to the environment due to their toxicity and formation of byproducts¹⁸. Furthermore, they normally pose significant issues like high operational cost and instability^{18,21}. Therefore, extensive efforts have been made for the sustainable production of more effective, stable and environmentally friendly bactericidal substances.

Zinc oxide nanostructures (ZnO) as excellent nanostructures-inspired biocides possess a wide range of properties that enable them to have superb antimicrobial potential and great biocompatibility²². Furthermore, some studies have presented convincing evidence that ZnO biocidal agents can be applied as disinfectant against water pollution²³. The antibacterial mechanisms are suggested to include the liberation of zinc ions from ZnO, disintegration of cell membrane upon contact with ZnO and Reactive Oxygen Species (ROS) formation²⁴. However, few studies have provided evidence on the ability of ZnO as biocides against field SRB consortium in the oil and gas sector. A recent study examined the MIC of stainless steel caused by SRB when treated with ZnO. It demonstrated that ZnO was able to inhibit the biofilm formation²⁵. Another study developed an inhibitor of zinc sorbate and showed that zinc sorbate had an excellent anti-biofilm formation activity against SRB consortium²⁶. It was also demonstrated that 250 µg/ml ZnO-chitosan inhibited SRB growth and sulfate reduction while reducing total organic carbon in seawater²⁷. They demonstrated that the inhibition of SRB biofilm formation in the presence of ZnO was concentration-dependent, although ZnO's behavior in the presence of sessile and planktonic cells was not provided. ZnO appears to be a proper choice as an inhibitor for the genera of SRB investigated so far. In addition, there is no report on the analysis of microbial community when ZnO is included in the media. In order to validate the use of ZnO as a biocide, more detailed information should be provided.

In the present study, an extremely corrosive SRB consortium obtained from the Iranian oil sector, was selected for lab measurements. This SRB consortium was continuously exposed to high concentrations of glutaraldehyde and isothiazolinone, and it has shown resistant and biofilm growth in the presence of these biocides in the pipelines. This SRB consortium was identified using 16S rRNA gene sequencing. Furthermore, the corrosion behavior of the SRB consortium on carbon steel coupons was investigated. Several techniques including confocal laser scanning microscopy (CLSM), scanning electron microscope (SEM), microbiological techniques, profilometry and electrochemical experiments were employed. ZnO was utilized to control MIC induced by the SRB consortium.

Materials and methods

Synthesis of ZnO

A chemical precipitation method was used as the synthesis route of ZnO according to a previous study²⁸. Typically, 4.0 g of $Zn(CH_3COO)_2 \cdot 2H_2O$ was added into 100 ml of deionized (DI) water in an erlenmeyer flask and placed on a hot plate magnetic stirrer with strong agitation at 30 °C for about 40 min. Following this step, 0.2 M of NaOH was added dropwise to the suspension and then the suspension was washed with water until the pH became neuter and lastly with ethanol. A furnace was utilized to dry the precipitate at 250 °C for 5 h and as a result $Zn(OH)_2$ was decomposed to ZnO. Prior to the experiment, a 10,000 ppm ZnO stock solution was prepared and ultrasonicated for 40 min using a probe sonicator (Elmasonic–Elma schmidbauer GmbH, Germany).

ZnO characterization

The synthesized ZnO was characterized by Dynamic light scattering (Zetasizer Nano, Malvern Instruments, United Kingdom), Fourier transform infrared spectroscopy (Vertex 70, Bruker, Germany) and scanning electron microscope (Model MIRA3, TESCAN, Czech Republic). For DLS and FTIR analysis, 5 mg of ZnO was dissolved in 5 mL of DI water and sonicated for 40 min before being analyzed.

SRB biofilm consortium, culture medium and coupons

The SRB consortium was enriched from Persian Gulf injection seawater obtained from an offshore oil and gas field in Iran. It seems that the consortium developed in the pipelines induces severe MIC and reduces the service life of pipelines and leads to catastrophes²⁹. Thus, control of the growth of the consortium could lead to the mitigation of MIC in the system. The medium composition for the growth of SRB consortium were according to NACE TM 0194-2014 (see Supplementary Table S1 online)³⁰.

Coin shaped C1018 carbon steel (CS) coupons (20 mm in diameter and 3 mm in height) were used for analysis of bacterial attachment³¹. Their elemental composition was (wt. %) 0.172 C, 0.154 Si, 0.347 Mn, 0.011 P, 0.007 S, 0.006 Cr, 0.02 Ni, 0.006 Al, 0.005 Co, 0.008 Cu and Fe balance. They were abraded with 200, 400 and 600 grit abrasive papers. The upper surface of coupons (surface area of 3.14 cm²) had exposure to the culture medium, but all the other surfaces were covered with epoxy resin. The oil surrounding the coupons was eliminated with acetone, rinsed with pure ethanol and sterilized under UV light for at least 20 min. In order to perform antibacterial analysis experiments, three sterilized coupons were placed at the bottom of each 1.5 L sterilized bioreactor. Bioreactors were filled with 1.5 L culture medium and then prepared SRB consortium was inoculated into each. Bioreactors were treated with 200 ppm ZnO as treated groups and bioreactors without ZnO were used as control. The initial planktonic cell count after inoculation was 10⁵ cells/mL. All the bioreactors were incubated at 30 °C for 1, 3, 7 and 14 days.

DNA extraction and microbial population assessments using metagenomics

The microbial populations grown in each bioreactor were identified using 16S rRNA gene sequencing³². The pellet of both planktonic and biofilm samples were obtained using centrifugation at 5000 g for 10 min. Then, in order to extract DNA of pellets, a DNeasy PowerBiofilm Kit (Qiagen, Germany) was employed according to the producer's directions. Later, the measurement of the produced DNA was performed using a Nanodrop spectrophotometer (Thermo scientific, Microvolume UV-Vis Spectrophotometer). The V3-V4 regions of 16S rRNA as the hypervariable regions were employed for amplification by PCR. Universal primers for amplification were 341F (5'CCTAYGGGRBGCASCAG3') and 806R (5' GGACTACNNGGGTATCTAAT 3') including barcodes³³. PCR amplification was implemented with 15 µL of Phusion® High-Fidelity PCR Master Mix (New England Biolabs); 2 µM of forward and reverse primers, and about 10 ng template DNA. The different stages of thermal cycling was including initial denaturation at 98 °C. Afterwards, 30 cycles of denaturation at 98 °C was performed for 10 s and then proceeded to anneal at 50 °C for 30 s. Subsequently, elongation occurred at 72 °C for 30 s and the last stage was extension at 72 °C for 5 min. Then, the products of PCR with appropriate size were investigated via the use of SYBR green and 2% gel agarose electrophoresis. Finally, the products of PCR had a purification stage with Qiagen Gel Extraction Kit (Qiagen, Germany). TruSeq® DNA PCR-Free Sample Preparation Kit (Illumina, USA) was utilized to create libraries of sequencing following the producer's directions. The quality of library was checked with Qubit® 2.0 Fluorometer (Thermo Scientific) and Agilent Bioanalyzer 2100 system. Finally, the library was sequenced on an Illumina NovaSeq platform and 250 bp paired-end reads were created. After filtering the sequences, the Silva Database was utilized based on RDP classifier algorithm for annotation of taxonomic information³⁴.

In order to assess phylogenetic relationship of each operational taxonomic unit (OTU) and the differences of the dominant species among different samples, multiple sequence alignment was implemented using the MUSCLE software (Version 3.8.31)³⁵. To analyze the bacterial population diversity and evenness, alpha diversity was applied through 2 indices including Shannon and Simpson. All the indices were computed using QIIME (Version 1.7.0) and visualized with R software (Version 2.15.3).

Bacterial enumeration

In order to acquire the counts of viable planktonic and sessile SRB cells in the control and ZnO treated bioreactors, serial dilution was utilized according to NACE TM 0194-2014³⁰. In brief, to estimate the count of viable sessile SRB cells, the biofilms on the coupons were washed three times with filtered-sterilized seawater. Then, the biofilms were removed from the coupons using a sterile loop and constant pipetting. Afterward, the removed biofilms were vortexed for 30 s and sonicated in a bath sonicator for 1 min until a cell suspension was obtained. Then, the serial dilution was implemented with three repetitions. Moreover, to estimate the count of planktonic SRB cells, 1 mL of culture medium was extracted from the bioreactors and serial dilution was conducted similar to sessile SRB cells.

Weight loss analyses and surface profilometry

The weight of the coupons was measured before and after immersion tests using a precise analytical balance (METTLER TOLEDO, Switzerland, readability 0.0001 g). According to ASTM G1-03, the Clark's solution was used to remove biofilms and corrosion products from coupon surfaces³⁶.

The weight loss results were interpreted as mg/cm². The calculation of corrosion rate was performed in mils per year (mpy) according to the equation below³⁷:

$$\text{Corrosion rate (mpy)} = \frac{W \times K}{A \times T \times D}$$

where W indicates coupon weight loss (g), K is 3.45×10^6 , A represents exposed surface area (cm²), T shows corrosion time (h), and D indicates density of carbon steel (g/cm³)³⁷.

Furthermore, a laser profilometer (LPM-D1, Fanavari Kahroba, Iran) was utilized to observe the topographic profile and measure the depth of corrosion pits of CS coupons.

Characterizations of biofilm morphology and corrosion products

For observation of biofilm morphology using SEM, CS coupons were retrieved from the bioreactors and immersed into 2.5% glutaraldehyde overnight. Subsequently, dehydration was implemented by ethanol with a concentration series (25%, 50%, 75%, 90% and 100%) and then coupons were maintained under dry nitrogen³⁸. Prior to SEM, gold sputtering was used to coat the coupons. Also, elemental composition of corrosion products was inspected with an energy-dispersive X-ray Spectroscopy (EDS).

In order to evaluate the performance of ZnO on developed biofilms, live/dead staining was carried out. The CS coupons were washed with filtered-sterilized seawater and stained with LIVE/DEAD® BacLight Kit based on its protocol. The observation of live/dead sessile cells was conducted using Confocal Laser Scanning Microscope (CLSM) (Leica, Germany).

Electrochemical tests and analyses

Working electrode for electrochemical tests was prepared by connecting a copper wire to each CS coupon and the coupon was covered with epoxy resin where only one surface had exposure. Saturated calomel electrode (SCE) was applied as the reference electrode and a graphite electrode was considered as the counter electrode. EIS and Linear Polarization Resistance (LPR) were implemented using an electrochemical station (IM6ex, Zahner-Elektrok, Germany). EIS measurements were conducted in a frequency between 10⁵ and 10⁻² with a sinusoidal

signal of 10 mV. Potentiodynamic polarization curves were measured at a scan rate of 0.5 mV/s within the potential range of -200 to 200 mV vs. Open circuit potential (OCP).

Statistical analysis

In order to normalize the data, Shapiro–Wilk method was employed for each variable. The statistical analyses were conducted with Student's *t*-test via OriginPro 2022 (V 9.9.0.225). The significance of statistical tests was deemed different when *p*-value was ≤ 0.05 . All experiments were conducted in three repetitions.

Ethics approval and consent to participate

Ethics approval is not applicable as this article does not describe any studies involving human participants or animals.

Results and discussion

Characterization of synthesized ZnO

The morphological features of the synthesized ZnO obtained by FE-SEM is shown in Fig. 1a. The prepared ZnO were often rod shape, and in some cases in the form of flower shape. Wahab et al. have shown that ZnO appear rod and flower shape at pH 7³⁹. Studies indicate that ZnO rod-like structures are more practical due to their

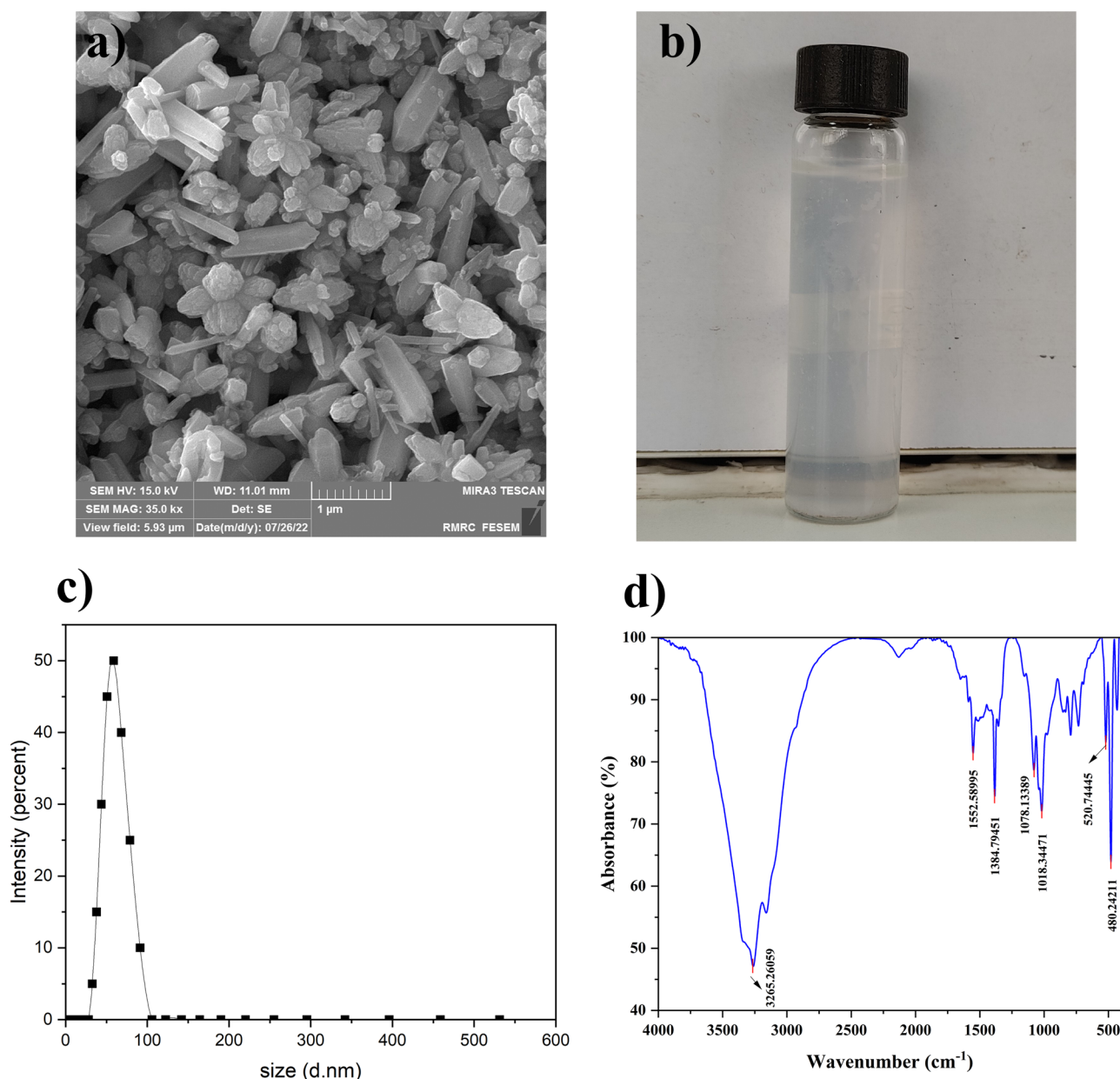


Fig. 1. Characterization of synthesized ZnO. (a) FE-SEM images of ZnO, (b) Photographic image of ZnO dispersed in seawater, (c) DLS plot of ZnO, and (d) FTIR spectral analysis of ZnO.

one-dimensional nanostructure⁴⁰. Moreover, studies illustrate that utilizing zinc acetate as a precursor could provide a stable and smoother ZnO aqueous suspension⁴¹. Figure 1b is a photographic image of ZnO aqueous suspension prepared in SW. Obvious observation displays that ZnO dispersibility is sufficient after a month (Fig. 1b). Moreover, DLS results show that the diameter of the synthesized ZnO is between 80 and 100 nm (Fig. 1c). Figure 1d displays the FTIR spectra of the synthesized ZnO. A broad absorption band at 3265 cm^{-1} and a peak at 1552 cm^{-1} demonstrate the O–H stretching vibrations of adsorbed water on the ZnO surface. Moreover, ZnO stretching modes are verified by the absorption band between 500 and 450 cm^{-1} ⁴².

Microbial community analysis

In order to investigate the changes in the microbial community in the presence and absence of ZnO, three different samples, including the sample directly taken from the pipeline (control0D) and the samples cultivated in the SRB bioreactors after 7 days in the absence (control7D) and presence of ZnO (ZnO7D) were evaluated. Herein, a total of 428,386 sequences from all three samples were generated from NGS analysis. After merging sequences, filtering tags and removing chimeras, 366,620 sequences were utilized for subsequent analysis and taxonomic identification.

The initial microbial population and both control and treated bioreactors were different after 7 days. Since the SRB consortium was obtained from the injection seawater of an oil and gas field, several microorganisms with critical ecological roles are numerously present in the samples. For instance, sulfate- and sulfur-reducing bacteria, acid-producing, thermophilic, halotolerant and halophilic bacteria are the main microbial groups existing in the oil reservoirs^{43,44}. Figure 2a represents the abundance of bacterial phyla. The data show that in the control0D, Desulfobacterota were the most frequent phylum. Afterwards, Proteobacteria, Firmicutes and Thermotogota had the highest quantities. Similarly, in the Control7D, Desulfobacterota had the highest dominance of 79.2%. Besides, Spirochaetota (9.9%), Firmicutes (7.6%) and Bacteroidota (2.3%) were found in great abundance. Moreover, inside the ZnO7D, Proteobacteria had the highest abundance of 89.8%. Subsequently, Firmicutes and Thermotogota had an abundance of 7.3% and 2.4%, respectively.

The microbial community of the genera is also presented in Fig. 2b. In the Control0D, the bacterial population consisted of microorganisms including *Halodesulfobivrio* (33.4%), *Geotoga* (10%), *Tepidibacter* (4.7%),

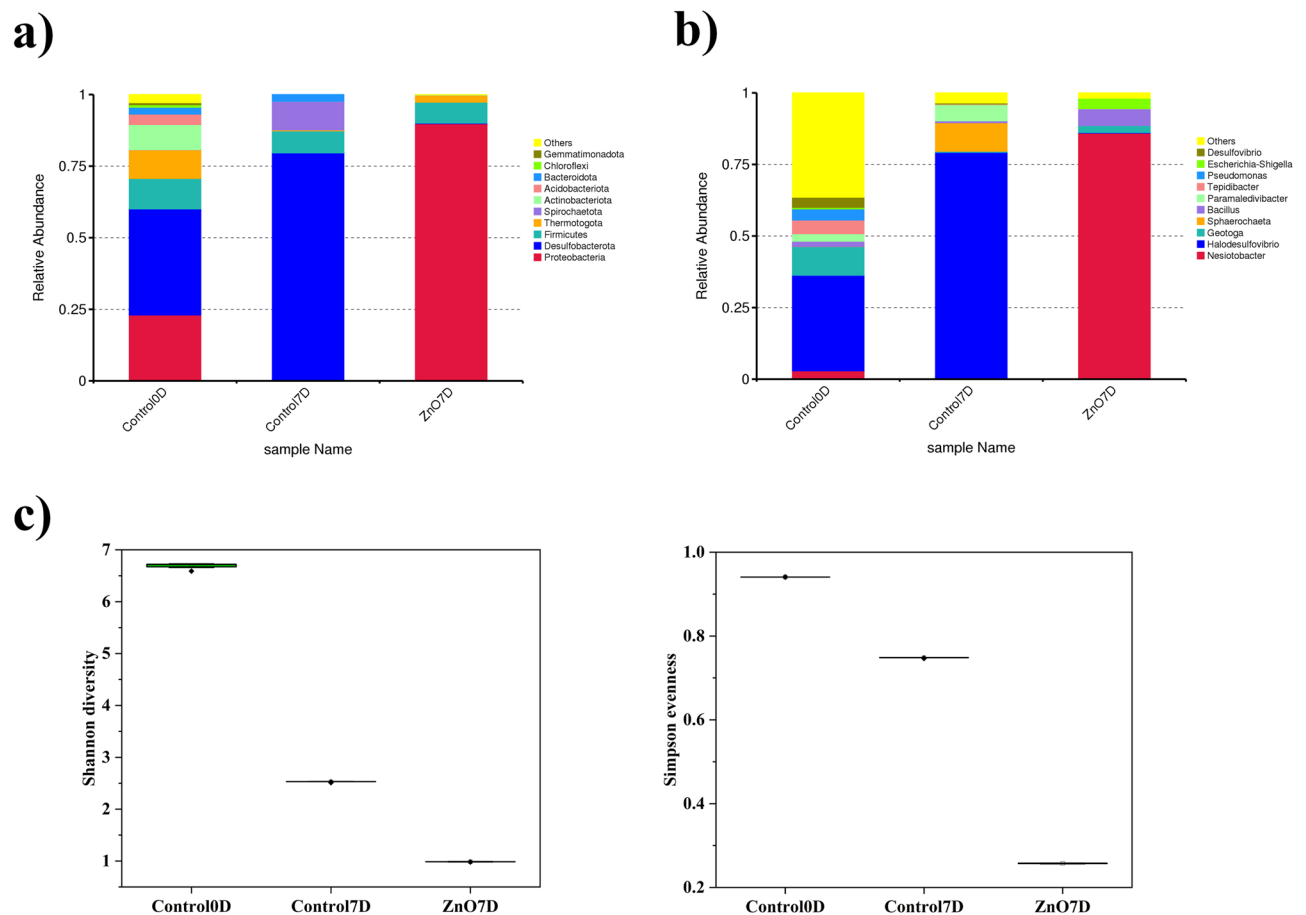


Fig. 2. Bar plots of diversity analysis at (a) the phylum level and (b) genus level. (c) alpha diversity of microbial populations. Boxes show the interquartile extent from the first and third quartiles, and the horizontal line in the box indicates the median.

Paramaledivibacter (2.6%), *Pseudomonas* (3.8%), *Desulfovibrio* (3.5%), *Nesiotobacter* (2.8%), *Prolixibacter* (1.9%), *Bacillus* (1.8%), *Pseudarthrobacter* (1.2%) and *Blastococcus* (1.2%), which accounted for 66.9% of the bacterial population.

The genus *Halodesulfovibrio* (SRB) was dominant in the initial consortium before conducting the test (Fig. 2b). Species of this genus are usually found in anoxic sediments of brackish and marine coasts⁴⁵. Due to the high salinity of injection water in Iran's offshore oil and gas fields, *Halodesulfovibrio* had the highest proportion in this SRB consortium relative to *Desulfovibrio* (Fig. 2b). In addition, the existence of moderately thermophilic bacteria such as *Geotoga* in various habitats like hot springs, hydrothermal vents and oil reservoirs led to their high abundance in the current consortium. The respiration of *Geotoga* is anaerobic, and they are able to ferment frequent substrates to form molecular hydrogen and cause the reduction of thiosulfate and elemental sulfur to hydrogen sulfide⁴⁶. Since thiosulfate could be produced in the dissimilatory sulfate reduction, *Geotoga* may also cause MIC⁴⁷.

Moreover, in the Control7D bioreactor, the genus *Halodesulfovibrio* had by far the highest percentage abundance of 78.9%. The genera *Sphaerochaeta* (9.9%), *Paramaledivibacter* (5.6%), *Prolixibacter* (1.4%) made up 16.9% of the bacterial population in the control bioreactor after 7 days (Fig. 2b). Although the relative abundance of some genera like *Sphaerochaeta* was markedly higher after 7 days, *Halodesulfovibrio* more than doubled through time and became the most predominant genus over time. Therefore, it is likely that *Halodesulfovibrio* correlates with MIC and it could be introduced as a potentially important corrosive genus.

The bacterial community in ZnO7D bioreactor was completely different from control and mostly included the genus *Nesiotobacter* (85.9%). Subsequently, the genera *Bacillus*, *Escherichia-Shigella*, *Geotoga* and *Clostridium sensu stricto1* were the most frequent (Fig. 2b). Studies have demonstrated that *Bacillus* is present in the biofilms on the metal surface and contributed to MIC⁴⁸. However, in this research, the corrosion rate inside the ZnO bioreactors was remarkably negligible compared to control bioreactors. Furthermore, the relative abundance of *Halodesulfovibrio* significantly dropped to below 1%, which was proof that ZnO had a strong inhibitory effect on *Halodesulfovibrio*. This, in turn, had an inhibitory impact on the corrosion rate and other genera existing in the consortium.

In addition, despite the inhibition of SRB consortium by ZnO, *Nesiotobacter* considerably increased inside the bioreactors containing ZnO. *Nesiotobacter* has been mostly found in marine and estuarine sediments, seawater, oil samples, wastewater treatment systems, and wetlands^{49,50}. *Nesiotobacter* is usually known for its high metabolic versatility and growth under various nutrient conditions⁵¹. For instance, identification and enrichment of some strains in an oil specimen and in a culture medium including hexadecane and other hydrocarbon compounds were reported⁵². Another property of this genus is its tolerance to toxic concentrations of heavy metals such as copper, lead, nickel and arsenic⁵³ and the present study showed the tolerance of this bacterium to ZnO.

The alpha diversity of microbial populations in the initial inoculum and control and ZnO bioreactors after 7 days of immersion is represented in Fig. 2c. The diversity index (Shannon) indicates the number of species in the bacterial population. The diversity of initial inoculum and control bioreactor was higher than ZnO bioreactors. Moreover, the Simpson index indicates that two randomly chosen individual species are the same. This index displayed that the initial bacterial community had a high even distribution (0.94). In the control and ZnO bioreactors, the even distribution was 0.74 and 0.25, respectively.

Analysis of planktonic and sessile SRB cells in the presence of ZnO

The growth rate of planktonic and sessile SRB cells in the presence and absence of ZnO was measured after 1, 3, 7 and 14 days of incubation. When ZnO were not included, planktonic SRB cell counts were 10^8 , 10^6 , 10^7 and 10^7 cells/mL during the incubation, respectively (Fig. 3a). However, inside the ZnO-containing bioreactors, the number of planktonic cells was 10^4 , 10^4 , 10^2 and 10^2 cells/mL, respectively (Fig. 3a). Thus, planktonic SRB cells

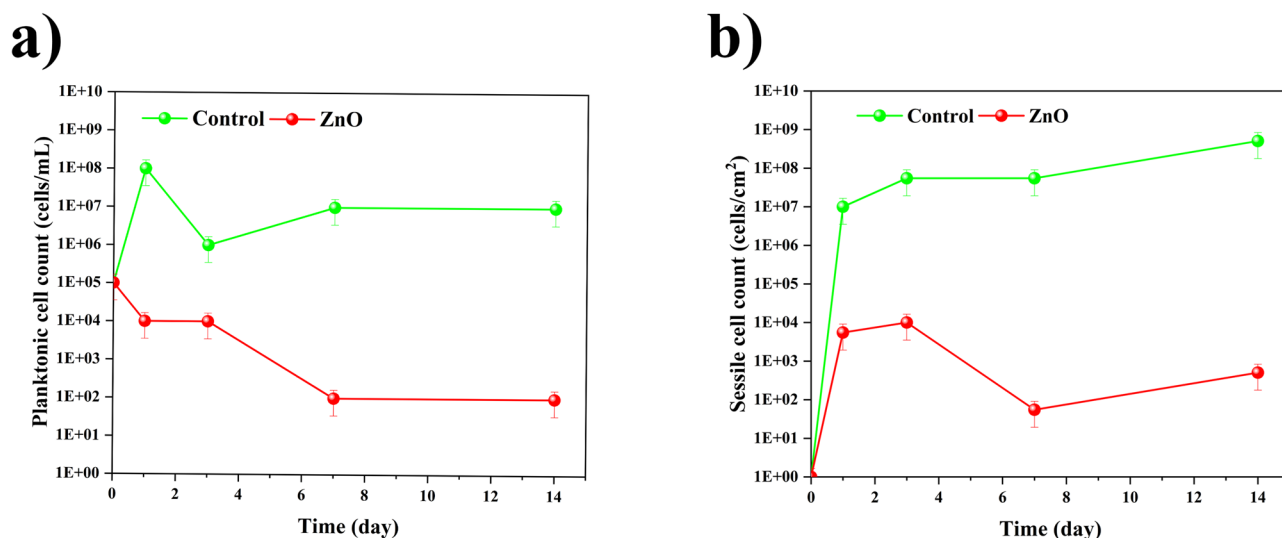


Fig. 3. (a) Planktonic and (b) sessile cell counts during the 14-day period of incubation.

counts significantly reduced in the presence of ZnO. Moreover, the enumeration of sessile SRB cells was estimated throughout the incubation period (Fig. 3b). In the absence of ZnO, sessile SRB cells counts were 10^7 , 10^7 , 10^7 and 10^8 cells/cm², respectively. However, inside the bioreactors containing ZnO, the counts of sessile SRB cells were 10^3 , 10^4 , 10^4 and 10^4 cells/cm², respectively. Moreover, As shown in Supplementary Fig. S1A online, treatment of SRB consortium with ZnO substantially affected the SRB cells' morphology and induced drastic damage on SRB cell membrane. However, in the absence of ZnO, the SRB consortium remained intact (see Supplementary Fig. S1B online). Herein, no obvious color changes were observed in the ZnO-treated bioreactors throughout the 14-day period (see Supplementary Fig. S2 online), indicating that SRB metabolism significantly reduced in the presence of ZnO. So far, numerous studies have reported the antibacterial property of ZnO against Gram-positive (*Staphylococcus aureus* and *Bacillus subtilis*) and Gram-negative (*Pseudomonas aeruginosa* and *Escherichia coli*) bacteria and its ability to inhibit biofilm formation^{54,55}. A study explored the antibacterial impact of rod-like ZnO on *B.subtilis* and *E.coli*. The counts of these bacteria were remarkably reduced due to dissolution of Zn²⁺ into the cytoplasm⁵⁶. Another experiment investigated the antibacterial mechanism of ZnO on *S.aureus*, showing that ZnO imposed serious harm on the cell membranes of bacteria. Consequently, reactive oxygen species (ROS) such as ·OH⁻, ·O₂⁻, and H₂O₂ were produced due to the antimicrobial impact of ZnO⁵⁷. It seems that negatively charged cell walls of bacteria are attached to positively charged nanoparticles due to electrostatic interactions. Forming a strong bond with membranes leads to the disruption of cell walls and increased permeability⁵⁸. In addition, it was reported that nanoparticles' morphologies influence their antimicrobial activity⁵⁹. ZnO had rod and flower-like morphologies in this research. Due to their high surface area, ZnO induced an effective antibacterial activity towards the SRB consortium. Recent reports have also confirmed the inhibitory effect of ZnO on the growth of SRB cells^{25,27}.

The surface morphologies of CS coupons in the abiotic and inoculated bioreactors could be observed in Figs. 4 and 5. In the abiotic bioreactors, there was almost no corrosion on the surface of coupons (Fig. 4a) and ZnO did not affect the surface morphology of coupons (Fig. 4b) after 14 days. In the inoculated bioreactors, sessile SRB cells were formed on the surface of control coupons after the first day (Fig. 5a). However, very few SRB cells were observed on the sample surfaces in the ZnO-treated bioreactors (Fig. 5b). Unlike in ZnO-treated samples, the biofilms were evenly formed on the surface of control coupons after the third day (Fig. 5c,d). During this period, corrosion products containing sulfur were seen only on the surface of the control but not ZnO-treated samples (see Supplementary Fig. S3A,B online). In SRB respiration, sulfate reduction yields bisulfide (HS⁻), which then combines with a proton to produce hydrogen sulfide (H₂S). HS⁻ can also react with Fe²⁺ to form iron sulfide as a corrosion product^{60,61}. As it can be seen in Fig. 5e–h after 7 and 14 days, notably more biofilms were formed in control samples compared to ZnO-treated samples. Inhibition of biofilm formation was evident when coupons were extracted from the bioreactor (see Supplementary Fig. S4 online). The results indicate that over the 14-day period, bacterial population declined significantly due to ZnO and little biofilm was formed on the surface of the coupons immersed in ZnO compared to the control bioreactors.

Moreover, CLSM images were used for visualization of biofilms on the surface of coupons. The biofilms developed on the coupons surfaces after 14 days of incubation are shown in Fig. 6. Living and dead sessile cells are shown in green and red spots, respectively. After 14 days, live sessile SRB cells covered the entire surface of coupons in the control bioreactors (Fig. 6a). However, in the presence of ZnO, the bacterial activity was dramatically reduced, as evidenced by the existence of red spots, though a number of sessile cells survived (Fig. 6b). Additionally, as shown from Fig. 6c, the mean intensity of biofilm layers represented the higher proportion

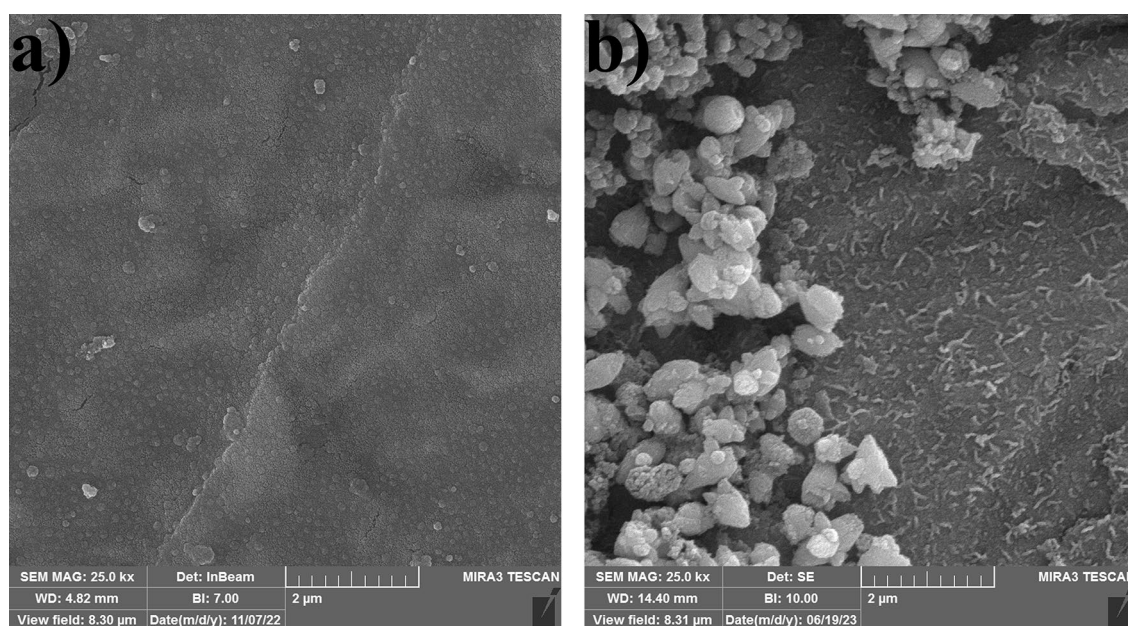


Fig. 4. FE-SEM images of abiotic bioreactors after 14 days of incubation: (a) Abiotic, (b) Abiotic + ZnO.

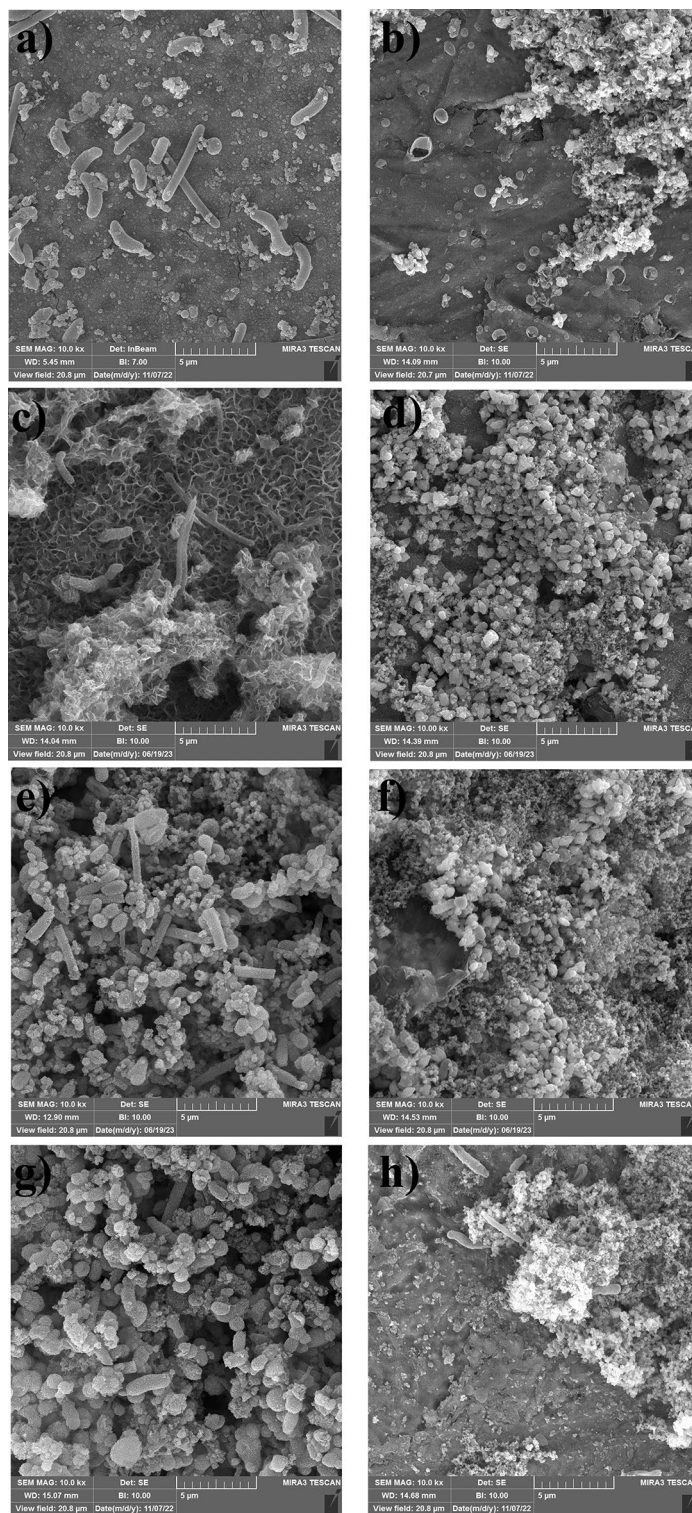


Fig. 5. FE-SEM images of SRB biofilms at different times. (a) control and (b) ZnO : 1 day , (c) control and (d) ZnO : 3 days, (e) control and (f) ZnO : 7 days, (g) control and (h) ZnO : 14 days.

of live sessile cells relative to dead sessile cells in the control bioreactors. Nevertheless, live sessile cells were considerably lower when ZnO were included. Furthermore, the population of dead sessile cells was increased, indicating that ZnO exerted a killing effect on sessile SRB cells. Overall, since the SRB consortium has shown resistance to high concentrations of glutaraldehyde and isothiazolinone, the introduction of ZnO could mitigate the resistance and remove the biofilms.

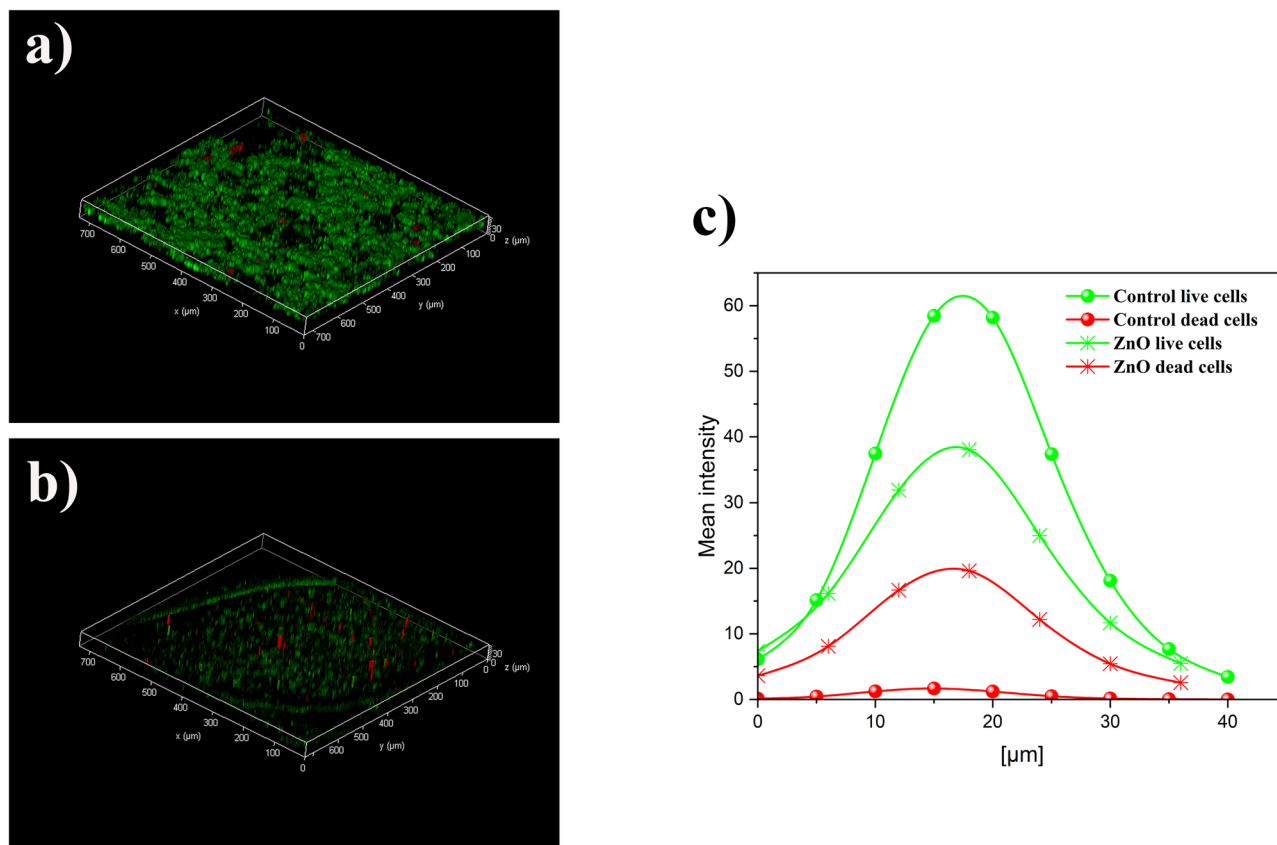


Fig. 6. CLSM images of biofilms on CS coupons after 14 days of immersion in the inoculated bioreactors: (a) control, (b) ZnO, and (c) mean intensity of live (green) and dead (red) cells.

Corrosion rate and surface analyses

The data on the weight loss of immersed coupons over 14 days are shown in Fig. 7. After the first day of incubation, the control and ZnO-treated bioreactors did not reveal any weight loss. This shows that most electrons necessary for cellular growth were taken from organic substances. However, after the third day, the weight loss of CS coupons was 0.95 mg/cm^2 (5.83 mpy) and 0.03 mg/cm^2 (0.19 mpy) in the control and ZnO-treated

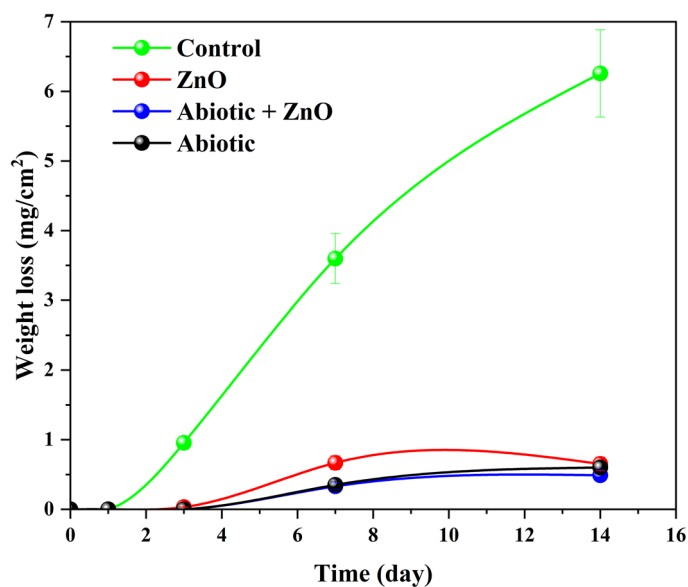


Fig. 7. Weight loss data of CS coupons in different abiotic and inoculated bioreactors during 14 days of immersion.

bioreactors, respectively. On this day, the weight loss of coupons in the control bioreactor was about 30 times higher than that of coupons immersed in the ZnO-treated bioreactor. After 7 days of incubation, the weight loss was 3.59 mg/cm² (9.426 mpy), indicating that severe corrosion occurred during this period. In the ZnO-treated bioreactor, CS coupons had a weight loss of 0.35 mg/cm² (0.91 mpy). Moreover, the weight loss of coupons in the control bioreactors was 6.25 mg/cm² (8.17 mpy), whereas the weight loss in the ZnO-treated bioreactors was 0.67 mg/cm² (0.87 mpy) after 14 days of incubation. This demonstrated that the corrosion rate in the bioreactor containing ZnO remained unchanged after the 7th day of incubation.

Weight loss of coupons placed in the abiotic media with and without ZnO was negligible (Fig. 7). No corrosion occurred after the first 3 days of incubation. After the 7th day, the weight loss was 0.35 mg/cm² (0.91 mpy) and 0.33 mg/cm² (0.86 mpy) in the abiotic and abiotic + ZnO bioreactors, respectively. The weight loss values changed slightly after 14 days reaching 0.6 mg/cm² (0.79 mpy) and 0.49 mg/cm² (0.64 mpy) in the abiotic and abiotic + ZnO bioreactors, respectively.

The surface morphology of CS coupons, when corrosion products and biofilms were cleaned, is presented in Fig. 8. Unlike ZnO-treated samples, severe corrosion was observed on the surface of control coupons after 7 and 14 days (Fig. 8a–d). The corrosion of the coupons in the control bioreactors was higher compared to the coupons immersed in the ZnO-treated bioreactors. This confirms that the SRB consortium induced serious damage on the coupon surfaces. The magnification of pit morphologies on the control CS coupons indicates that the pits are nearly circular, with the widest pit being about 18.34 μm (Fig. 8e).

The surface morphology and pit depth profiles after the coupons biofilm removal were scanned and illustrated in Fig. 9. Moreover, photographic images of coupons' surfaces from control and ZnO-treated bioreactors during the 14 days of immersion are presented in Supplementary Fig. S5 online. Before conducting the test, a blank CS coupon had a maximum pit depth value of − 10.0 μm and mean depth of − 4.99 μm (see Supplementary Fig. S6 online). As previously reported, large localized corrosion was found when coupons were exposed to the SRB consortium⁶². After 7 days of incubation without treatment, the maximum pit depth increased to − 32.48 μm and the mean depth of pits was − 18.98 μm (Fig. 9a). However, when ZnO were added to the bioreactor, the maximum pit depth was − 14.19 μm and the mean depth of pits on the coupon surfaces was − 8.70 μm (Fig. 9b). On the 14th day, the maximum pit depth of control coupon increased to − 68.3 μm and the mean depth pits increased to − 37.7 μm (Fig. 9c). In the bioreactors containing ZnO, maximum pit depth was − 18.12 μm and the mean depth of corrosion pits was − 9.09 μm (Fig. 9d). Based on the results obtained, the pitting corrosion of CS coupons immersed in the control bioreactors markedly increased during the incubation time. Previous investigations also verified the intensification of pitting corrosion⁶³. Therefore, the addition of ZnO substantially reduced the pitting corrosion caused by the SRB consortium.

Electrochemical analyses

The SRB consortium generally impacts the electrochemical properties of CS coupons. As a result, electrochemical experiments were conducted on days 1, 3, 7 and 14 to assess microbial activities of the SRB consortium. Polarization resistance (R_p) data showed that in the abiotic coupons, with or without ZnO, the R_p values were 11.5 kΩ cm² and 9.5 kΩ cm² after 14 days of immersion, which were almost similar. The R_p of control coupons was 0.63 kΩ cm² after 14 days, revealing that they had the highest corrosion rates. However, the R_p of coupons treated with ZnO was 72.5 kΩ cm² which was far higher than the control coupons. This meaningful difference in R_p of control and ZnO coupons exhibits the continued protection impact of ZnO and verifies the weight loss and pit depth data. Furthermore, the lowest R_p in the control coupons is due to the early biofilm formation and growth of SRB consortium which facilitated MIC from the starting day. Similar data on the low R_p as a consequence of biofilm development was previously reported⁶⁴.

The EIS data including Nyquist and Bode plots are described in Fig. 10. In the abiotic bioreactors, the radii of capacitive arcs in Nyquist plots revealed no decreases with time (Fig. 10a). Two time constants in the middle- and low- frequency regions were identified in the Bode phase plots (Fig. 10b). In the abiotic + ZnO bioreactors, the size of the semicircle revealed a significant reduction after the first day and then remained almost unchanged after 7 days of incubation (Fig. 10c). Moreover, the phase angle diagram indicated no substantial changes in the corresponding Bode phase plots (Fig. 10d). For the control bioreactors, the radii of capacitive arcs in the Nyquist diagram remarkably reduced following the first day and then gradually decreased with the passing of time, indicating that corrosion rate was accelerated after the first day of immersion (Fig. 10e). In the Bode phase plots, the values of the phase angle displayed a reduction in the low frequency region (Fig. 10f). It was proposed that the corrosion resistance of control CS coupons declined substantially as a result of the corrosive behavior of SRB consortium⁶⁵. When ZnO was added to the bioreactors, the radii of capacitive arcs did not exhibit a significant decrease with time and the phase angle plot did not change through time (Fig. 10g,h).

To fit the EIS results in Fig. 10, ZView software was used and the electrical equivalent circuits in series were recommended in Supplementary Fig. S7 online. A two time-constant model was used to fit the EIS results acquired from the control, ZnO and abiotic bioreactors. In the electrical equivalent circuit, R_s indicates the solution resistance. Q_f and R_f are the capacitance and resistance of the surface film and biofilm, respectively. Q_{dl} and R_{ct} are the capacitive and charge transfer resistance of the electric double layer. The constant phase element (CPE, Q) was employed to substitute for the capacitance C due to its nonideal behavior on the surface of CS coupons.

The results of fitting parameters acquired from EIS experiments are shown in Table 1. In the abiotic bioreactors, the R_{ct} value remained relatively stable as it decreased from 10011.67 to 8155.38 Ω cm², and C_{dl} values increased from 396.52 to 530 μF cm⁻². Moreover, in the abiotic bioreactors containing ZnO, the R_{ct} values gradually declined to 10113.78 Ω cm² and C_{dl} values were 228.65 μF cm⁻² after 14 days of incubation. In addition, in the control bioreactors, the R_{ct} values dropped markedly from 2374.72 to 638.17 Ω cm², indicating that the charge transfer resistance was significantly small from the starting day. The C_{dl} values grew sharply from 9292.04

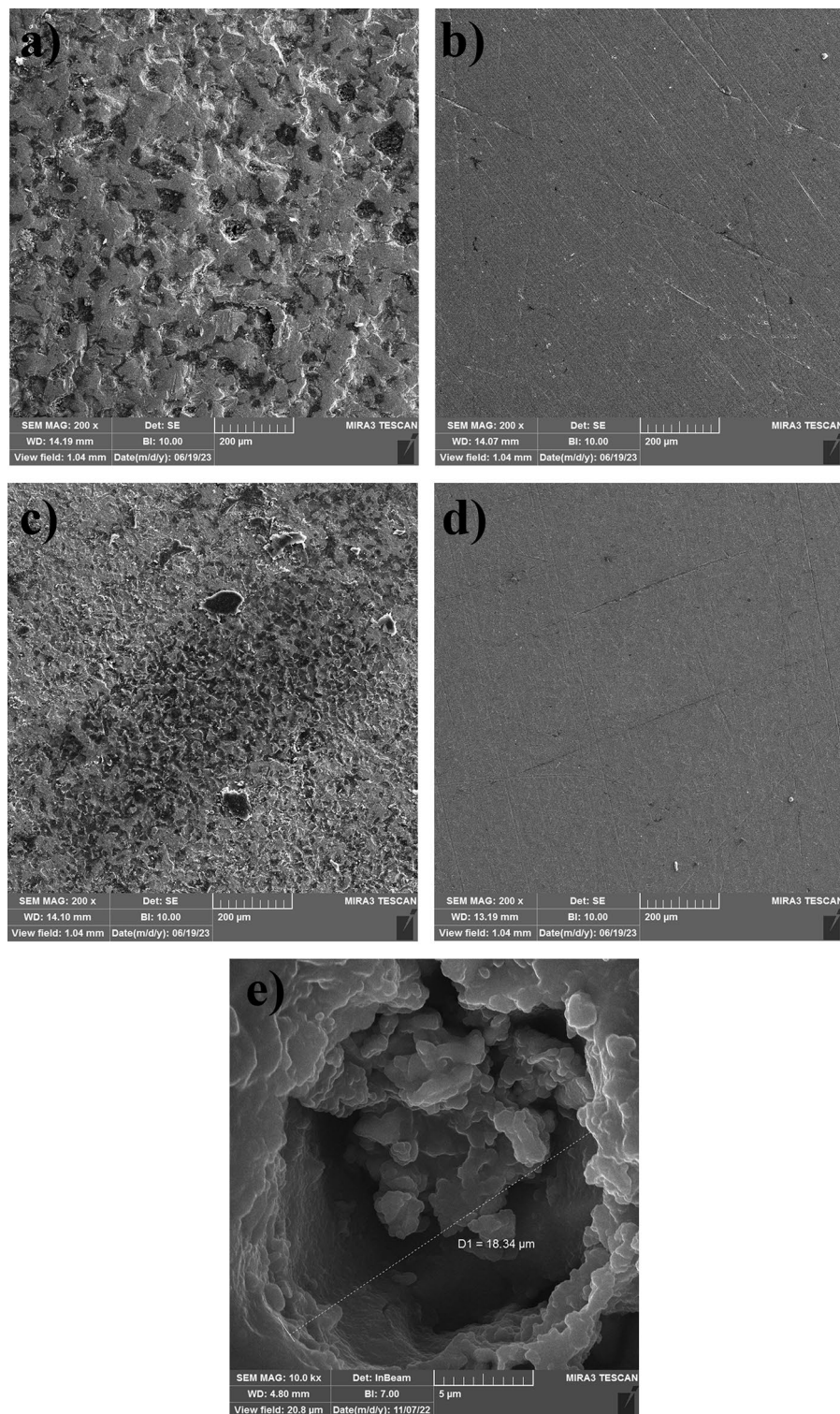


Fig. 8. FE-SEM images of CS coupons when surface was cleaned at various times. **(a)** control and **(b)** ZnO : 7 days, **(c)** control and **(d)** ZnO : 14 days, **(e)** magnified pit morphology of control coupons.

to $115047.11 \mu\text{F cm}^{-2}$ with the evolution of time. In the ZnO bioreactors, the R_{ct} values change was relatively smaller and reached $65700.16 \Omega \text{ cm}^2$. Plus, the C_{dl} value was $375.98 \mu\text{F cm}^{-2}$ after 14 days of immersion time. This demonstrated that the corrosion resistance of coupons in the ZnO bioreactors was notably higher than in the control bioreactors and that ZnO totally inhibited the corrosion of CS coupons. Besides the R_{ct} data, R_f and C_f values did not change in the abiotic bioreactors without or containing ZnO, showing that the resistance of

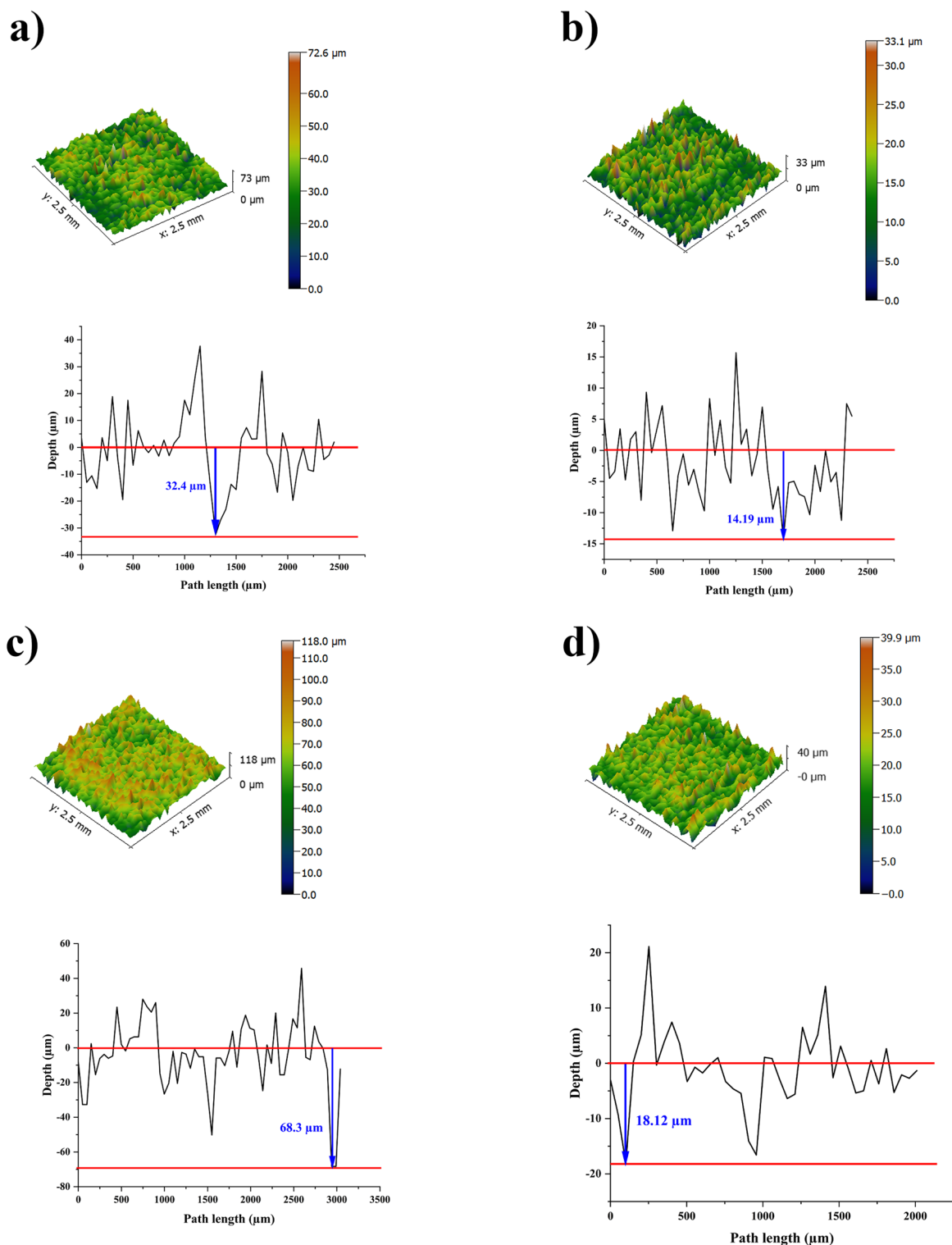


Fig. 9. Pitting profiles of CS coupons. (a) control and (b) ZnO : 7 days, (c) control and (d) ZnO : 14 days.

surface film did not change over time. In the control bioreactors, the R_f values markedly decreased from 115.69 to only $0.65 \Omega \text{ cm}^2$ and the C_f value increased to $6136.44 \mu\text{F cm}^{-2}$ after 14 days of immersion.

The polarization curves of the CS coupons in the abiotic and inoculated bioreactors containing ZnO are shown in Fig. S8. The corrosion potentials (E_{corr}), current densities (i_{corr}) and Tafel parameters are also listed in Table 2. The abiotic bioreactors indicated negligible corrosion current densities. Moreover, the corrosion potentials did not change substantially in the abiotic bioreactors, which is shown in Supplementary Fig. S8A online. The data also exhibited that ZnO did not augment the corrosion rate of CS coupon. In the control bioreactors, i_{corr} increased from 2.9 to $56.2 \mu\text{A/cm}^2$ during 14 days of incubation, indicating that the coupons inside the control bioreactors had by far the highest corrosion rate. Plus, E_{corr} was the lowest in the control bioreactors, showing

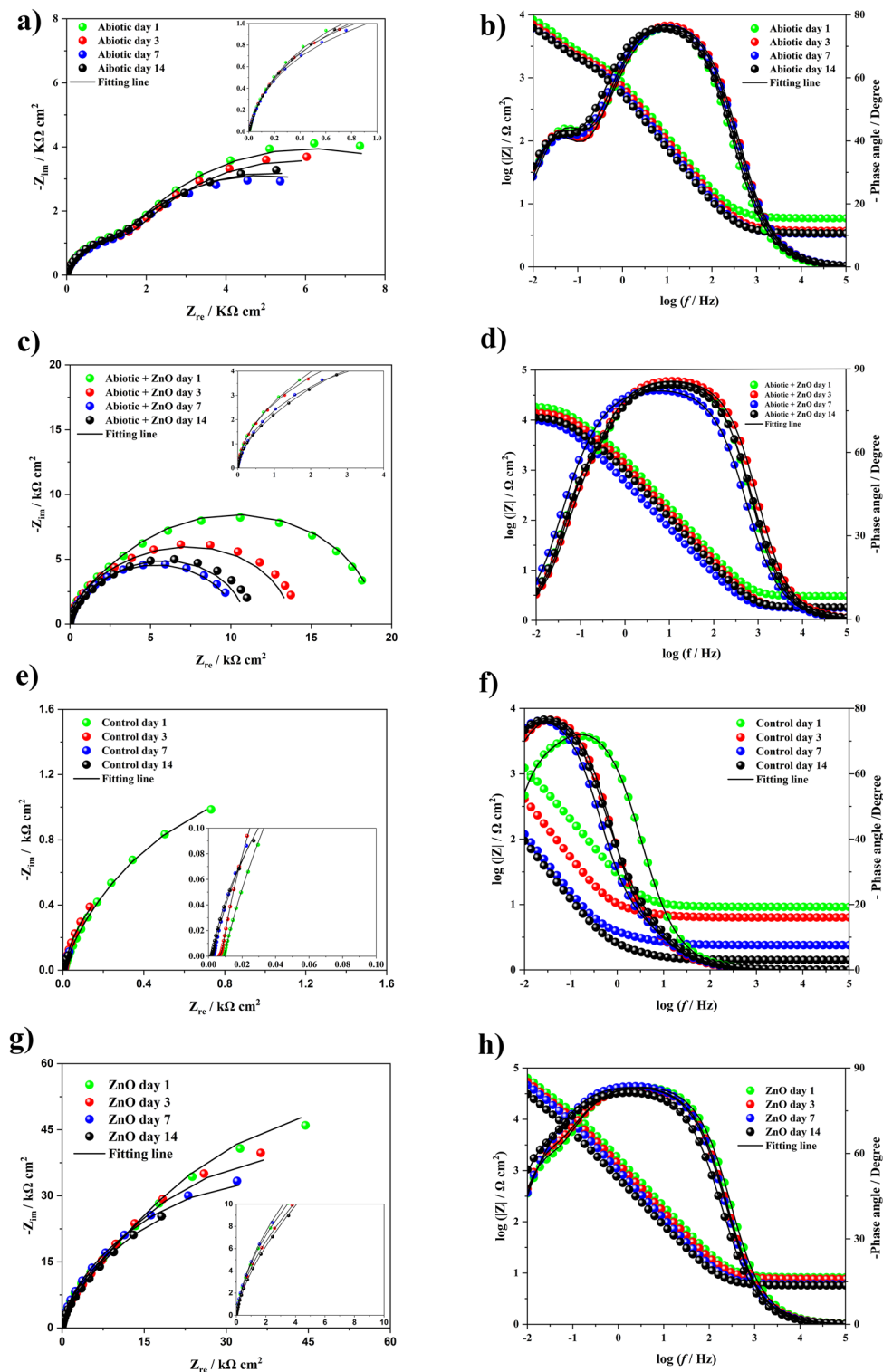


Fig. 10. EIS data including Nyquist and Bode phase plots CS coupons in different bioreactors at various exposure times: (a,b) : Abiotic, (c,d) : Abiotic + ZnO, (e,f) : Control; (g,h) : ZnO.

the highest thermodynamic tendency for corrosion. This is also shown in Supplementary Fig. S8B online. The data, along with the EIS results, showed that the impedance of CS coupons drastically reduced in the presence of the SRB consortium biofilms (Fig. 10e). This gave rise to the occurrence of corrosion and numerous corrosion pits were formed during 14 days of immersion, as indicated in Fig. 8a,c. However, i_{corr} was significantly lowered from 0.85 to 0.48 $\mu\text{A}/\text{cm}^2$ in the ZnO-treated bioreactor. As a result, it was proved that the excellent inhibition efficiency of ZnO was evident. Furthermore, as shown in Supplementary Fig. S8C online, the corrosion

Bioreactors	Time (day)	R_s ($\Omega \text{ cm}^2$)	R_f ($\Omega \text{ cm}^2$)	C_f ($\mu\text{F cm}^{-2}$)	R_{ct} ($\Omega \text{ cm}^2$)	C_{dl} ($\mu\text{F cm}^{-2}$)
Control	1	9.21	115.69	2097.06	2374.72	9292.04
	3	6.35	1.38	3432.79	2067.12	26,724.24
	7	2.39	0.94	4933.93	881.05	94,925.55
	14	1.42	0.65	6136.44	638.17	115,047.11
ZnO	1	8.2	12,942.02	60.59	95,678.42	197.03
	3	7.68	8458.45	78.26	83,584.11	224.18
	7	6.10	7710.78	125.61	68,907.52	235.36
	14	5.75	6860.02	130.20	65,700.16	375.98
Abiotic	1	5.88	1518.53	79.23	10,011.67	396.52
	3	3.71	1467.00	90.82	9080.47	486.18
	7	3.33	1341.95	101.72	7231.94	523.09
	14	3.39	1411.07	118.68	8155.38	530.28
Abiotic + ZnO	1	2.89	2623.26	146.25	16,383.33	151.42
	3	1.68	2449.19	170.71	11,792.24	192.11
	7	1.67	1260.26	258.08	9249.42	234.97
	14	1.73	1416.10	224.21	10,113.78	228.65

Table 1. Fitting parameters acquired from the EIS experiments in control, ZnO and abiotic coupons.

Bioreactors	Time (day)	i_{corr} ($\mu\text{A/cm}^2$)	E_{corr} (mV vs SCE)	β_a (mV/dec)	β_c (mV/dec)
Control	1	2.9	-670	77	129
	3	8.25	-756	119	97
	7	30.7	-774	158	87
	14	56.2	-842	114	92
ZnO	1	0.85	-807	156	69
	3	0.36	-750	98	102
	7	0.15	-776	96	98
Abiotic	14	0.48	-754	145	94
	1	2.54	-711	44	156
	3	1.38	-764	179	73
Abiotic + ZnO	7	0.38	-773	93	85
	14	0.44	-743	154	92
	1	1.85	-736	57	199
	3	0.97	-778	92	80
Abiotic + ZnO	7	0.37	-766	87	89
	14	0.32	-737	91	112

Table 2. Polarization parameters derived from the Tafel analysis of coupons in the bioreactors with and without treatment.

densities and the corrosion potentials did not change significantly over time. The values in the ZnO bioreactors were approximately similar to those in the abiotic bioreactors. It can be concluded that adding ZnO effectively inhibited the pitting corrosion of CS coupons. These findings were completely in line with the corrosion pit results (Fig. 8b,d) and EIS data (Fig. 10g). Consequently, the polarization findings were consistent with the data of corrosion pit analysis and EIS data.

Conclusion

In the current research, the corrosion behavior of a marine SRB consortium and the inhibition of MIC in the presence of ZnO were investigated. Metagenomics analysis showed that *Halodesulfobivrio* was the most dominating genus. Thus, *Halodesulfobivrio* could be related to MIC and potentially an important corrosive genus in a marine SRB consortium. However, in the ZnO-treated bioreactors, *Halodesulfobivrio* sharply reduced to less than 1%. It was also shown that a major change from a highly corrosive SRB consortium in the control bioreactors to a significantly lower corrosive consortium in the ZnO-treated bioreactors occurred. Furthermore, A considerable reduction in the growth rate of planktonic and sessile SRB cells within the ZnO-treated bioreactors was witnessed and SEM images exhibited severe harm to the cells. The corrosion rate of CS coupons in the control bioreactors reached 8.17 mpy during a 14-day period. However, in the ZnO-treated bioreactors, the inhibition of corrosion rate was approximately 90%. SEM images demonstrated that the surface of CS coupons were covered with pits

in the control bioreactors, whereas no pits were observed in the ZnO-treated bioreactors. Overall, our study showed that *Halodesulfobivrio* should be taken into account in marine oilfield systems. Moreover, ZnO could be considered an excellent choice to inhibit MIC induced by *Halodesulfobivrio*.

Data availability

All data are included in the manuscript and additional information, and further queries about sharing data can be directed to the corresponding author.

Received: 1 May 2024; Accepted: 20 August 2024

Published online: 22 August 2024

References

- Qian, H. *et al.* Investigation of microbiologically influenced corrosion inhibition of 304 stainless steel by D-cysteine in the presence of *Pseudomonas aeruginosa*. *Bioelectrochemistry* **143**, 107953 (2022).
- Liu, H., Cheng, Y. F., Xu, D. & Liu, H. Effect of iron oxidizing bacteria biofilm on corrosion inhibition of imidazoline derivative in CO₂-containing oilfield produced water with organic carbon source starvation. *J. Electrochem. Soc.* **165**, C354 (2018).
- Makama, Z., Celikkol, S., Ogawa, A., Gaylarde, C. & Beech, I. The issue with using DNA profiling as a sole method for investigating the role of marine biofilms in corrosion of metallic materials. *Int. Biodeterior. Biodegrad.* **135**, 33–38 (2018).
- Tuck, B., Watkin, E., Somers, A. & Machuca, L. A critical review of marine biofilms on metallic materials. *Npj Mater. Degrad.* **6**, 25 (2022).
- Bhat, S., Kumar, B., Prasad, S. & Katarki, M. Failure of a new 8-in pipeline from group gathering station to central tank farm. *Mater. Perf.* **50**, 50–54 (2011).
- Jia, R., Yang, D., Xu, J., Xu, D. & Gu, T. Microbiologically influenced corrosion of C1018 carbon steel by nitrate reducing *Pseudomonas aeruginosa* biofilm under organic carbon starvation. *Corros. Sci.* **127**, 1–9 (2017).
- Sivakumar, K. *et al.* Salinity-mediated increment in sulfate reduction, biofilm formation, and quorum sensing: A potential connection between quorum sensing and sulfate reduction?. *Front. Microbiol.* **10**, 188 (2019).
- Vigneron, A. *et al.* Complementary microorganisms in highly corrosive biofilms from an offshore oil production facility. *Appl. Environ. Microbiol.* **82**, 2545–2554 (2016).
- Li, X. *et al.* Analysis of bacterial community composition of corroded steel immersed in Sanya and Xiamen seawaters in China via method of Illumina MiSeq sequencing. *Front. Microbiol.* **8**, 1737 (2017).
- Muyzer, G. & Stams, A. J. The ecology and biotechnology of sulphate-reducing bacteria. *Nat. Rev. Microbiol.* **6**, 441–454 (2008).
- Cetin, D. & Aksu, M. L. Corrosion behavior of low-alloy steel in the presence of *Desulfotomaculum* sp. *Corros. Sci.* **51**, 1584–1588 (2009).
- Anandkumar, B., Choi, J. H., Venkatachari, G. & Maruthamuthu, S. Molecular characterization and corrosion behavior of thermophilic (55 C) SRB *Desulfotomaculum kuznetsovii* isolated from cooling tower in petroleum refinery. *Mater. Corros.* **60**, 730–737 (2009).
- Vlasov, D. Y. *et al.* The corrosive activity of microorganisms isolated from fouling of structural materials in the coastal zone of the Barents sea. *Appl. Biochem. Microbiol.* **59**, 425–437 (2023).
- Galushko, A. & Kuever, J. *Paradesulfobivrio*. *Bergey's Manual of Systematics of Archaea and Bacteria*, 1–5 (2015).
- Galushko, A. & Kuever, J. *Desulfotomaculum*. *Bergey's Manual of Systematics of Archaea and Bacteria*, 1–6 (2015).
- Jia, R., Yang, D., Li, Y., Xu, D. & Gu, T. Mitigation of the *Desulfobivrio vulgaris* biofilm using alkyldimethylbenzylammonium chloride enhanced by D-amino acids. *Int. Biodeterior. Biodegrad.* **117**, 97–104 (2017).
- Xu, J., Jia, R., Yang, D., Sun, C. & Gu, T. Effects of D-Phenylalanine as a biocide enhancer of THPS against the microbiologically influenced corrosion of C1018 carbon steel. *J. Mater. Sci. Technol.* **35**, 109–117 (2019).
- Rasool, K. *et al.* Screening the growth inhibition mechanism of sulfate reducing bacteria by chitosan/lignosulfonate nanocomposite (CS@LS) in seawater media. *J. Environ. Chem. Eng.* **9**, 106624 (2021).
- Batista, J. *et al.* In situ corrosion control in industrial water systems. *Biodegradation* **11**, 441–448 (2000).
- Vance, I. & Thrasher, D. R. Reservoir souring: Mechanisms and prevention. *Pet. Microbiol.*, 123–142 (2005).
- Little, B. *et al.* Microbially influenced corrosion—Any progress?. *Corros. Sci.* **170**, 108641 (2020).
- Qi, K., Cheng, B., Yu, J. & Ho, W. Review on the improvement of the photocatalytic and antibacterial activities of ZnO. *J. Alloys Comp.* **727**, 792–820 (2017).
- Dimapilis, E. A. S., Hsu, C.-S., Mendoza, R. M. O. & Lu, M.-C. Zinc oxide nanoparticles for water disinfection. *Sustain. Environ. Res.* **28**, 47–56 (2018).
- Sirelkhatim, A. *et al.* Review on zinc oxide nanoparticles: Antibacterial activity and toxicity mechanism. *Nano-micro Lett.* **7**, 219–242 (2015).
- Zhang, Y. *et al.* Microbiologically influenced corrosion behavior of 304 stainless steel in ZnO nanofluids. *Corros. Rev.* (2023).
- Parthipan, P., Cheng, L., Dhandapani, P. & Rajasekar, A. Metagenomics diversity analysis of sulfate-reducing bacteria and their impact on biocorrosion and mitigation approach using an organometallic inhibitor. *Sci. Total Environ.* **856**, 159203 (2023).
- Rasool, K. *et al.* “Green” ZnO-interlinked chitosan nanoparticles for the efficient inhibition of sulfate-reducing bacteria in inject seawater. *ACS Sustain. Chem. Eng.* **6**, 3896–3906 (2018).
- Akpomie, K. G., Ghosh, S., Gryzenhout, M. & Conradie, J. One-pot synthesis of zinc oxide nanoparticles via chemical precipitation for bromophenol blue adsorption and the antifungal activity against filamentous fungi. *Sci. Rep.* **11**, 8305 (2021).
- Abedi, S. S., Abdolmaleki, A. & Adibi, N. Failure analysis of SCC and SRB induced cracking of a transmission oil products pipeline. *Eng. Failure Anal.* **14**, 250–261 (2007).
- NACE. (NACE International Houston, TX, 2014).
- Xu, D. & Gu, T. Carbon source starvation triggered more aggressive corrosion against carbon steel by the *Desulfobivrio vulgaris* biofilm. *Int. Biodeterior. Biodegrad.* **91**, 74–81 (2014).
- Diaz-Mateus, M. A., Salgar-Chaparro, S. J., Machuca, L. L. & Farhat, H. Effect of deposit chemistry on microbial community structure and activity: Implications for under-deposit microbial corrosion. *Front. Microbiol.* **14**, 1089649 (2023).
- Salgar-Chaparro, S. J., Darwin, A., Kaksonen, A. H. & Machuca, L. L. Carbon steel corrosion by bacteria from failed seal rings at an offshore facility. *Sci. Rep.* **10**, 12287 (2020).
- Quast, C. *et al.* The SILVA ribosomal RNA gene database project: Improved data processing and web-based tools. *Nucleic Acids Res.* **41**, D590–D596 (2012).
- Edgar, R. C. MUSCLE: Multiple sequence alignment with high accuracy and high throughput. *Nucleic Acids Res.* **32**, 1792–1797 (2004).
- Standard, A. G1-03. Standard Practice for preparing, cleaning, and evaluating corrosion test specimens, Annual Book of ASTM Standards **3**, 17–25 (2003).
- Kearns, J. R., Kearns, J. R. & Little, B. J. *Microbiologically Influenced Corrosion Testing* Vol. 1232 (ASTM International, 1994).

38. Phan, H. C., Blackall, L. L. & Wade, S. A. Effect of multispecies microbial consortia on microbially influenced corrosion of carbon steel. *Corros. Mater. Degrad.* **2**, 133–149 (2021).
39. Wahab, R., Ansari, S., Kim, Y. S., Song, M. & Shin, H.-S. The role of pH variation on the growth of zinc oxide nanostructures. *Appl. Surf. Sci.* **255**, 4891–4896 (2009).
40. Moezzi, A., McDonagh, A. M. & Cortie, M. B. Zinc oxide particles: Synthesis, properties and applications. *Chem. Eng. J.* **185**, 1–22 (2012).
41. Bahadur, H., Srivastava, A., Sharma, R. & Chandra, S. Morphologies of sol–gel derived thin films of ZnO using different precursor materials and their nanostructures. *Nanoscale Res. Lett.* **2**, 469–475 (2007).
42. Lepot, N. *et al.* Synthesis of ZnO nanorods from aqueous solution. *Mater. Lett.* **61**, 2624–2627 (2007).
43. Li, X.-X. *et al.* Microbiota and their affiliation with physiochemical characteristics of different subsurface petroleum reservoirs. *Int. Biodeterior. Biodegrad.* **120**, 170–185 (2017).
44. Rajbongshi, A. & Gogoi, S. B. A review on anaerobic microorganisms isolated from oil reservoirs. *World J. Microbiol. Biotechnol.* **37**, 111 (2021).
45. Shivani, Y., Subhash, Y., Sasikala, C. & Ramana, C. V. Halodesulfobrio spirochaetisodalis gen. nov. sp. Nov. and reclassification of four Desulfobrio spp. *Int. J. System. Evol. Microbiol.* **67**, 87–93 (2017).
46. Semenova, E., Grouzdev, D., Tourova, T. & Nazina, T. Physiology and genomic characteristics of Geotoga petraea, a bacterium isolated from a low-temperature petroleum reservoir (Russia). *Microbiology* **88**, 662–670 (2019).
47. Qian, Z., Tianwei, H., Mackey, H. R., van Loosdrecht, M. C. & Guanghao, C. Recent advances in dissimilatory sulfate reduction: From metabolic study to application. *Water Res.* **150**, 162–181 (2019).
48. Selvaraj, C., Sivakamavalli, J., Vaseeharan, B., Singh, P. & Singh, S. K. Examine the characterization of biofilm formation and inhibition by targeting SrtA mechanism in *Bacillus subtilis*: A combined experimental and theoretical study. *J. Mol. Model.* **20**, 1–15 (2014).
49. Hosoya, S. & Yokota, A. *Pseudovibrio japonicus* sp. nov., isolated from coastal seawater in Japan. *Int. J. System. Evol. Microbiol.* **57**, 1952–1955 (2007).
50. Romano, S. Ecology and biotechnological potential of bacteria belonging to the genus *Pseudovibrio*. *Appl. Environ. Microbiol.* **84**, e02516–02517 (2018).
51. Versluis, D. *et al.* Comparative genomics highlights symbiotic capacities and high metabolic flexibility of the marine genus *Pseudovibrio*. *Genome Biol. Evol.* **10**, 125–142 (2018).
52. Silva, T., Verde, L., Neto, E. S. & Oliveira, V. Diversity analyses of microbial communities in petroleum samples from Brazilian oil fields. *Int. Biodeterior. Biodegrad.* **81**, 57–70 (2013).
53. Bauvais, C. *et al.* Sponging up metals: Bacteria associated with the marine sponge *Spongia officinalis*. *Mar. Environ. Res.* **104**, 20–30 (2015).
54. Sánchez-López, E. *et al.* Metal-based nanoparticles as antimicrobial agents: An overview. *Nanomaterials* **10**, 292 (2020).
55. Rosenberg, M. *et al.* Selective antibiofilm properties and biocompatibility of nano-ZnO and nano-ZnO/Ag coated surfaces. *Sci. Rep.* **10**, 13478 (2020).
56. Chang, J. S., Chong, M. N. & Ocon, J. D. Determining the structure-antibacterial properties relationship and bacterial inactivation kinetics in different morphological-controlled ZnO nanoarchitectures for wastewater applications. *J. Environ. Chem. Eng.* **9**, 106646 (2021).
57. Lakshmi Prasanna, V. & Vijayaraghavan, R. Insight into the mechanism of antibacterial activity of ZnO: Surface defects mediated reactive oxygen species even in the dark. *Langmuir* **31**, 9155–9162 (2015).
58. Stensberg, M. C. *et al.* Toxicological studies on silver nanoparticles: Challenges and opportunities in assessment, monitoring and imaging. *Nanomedicine* **6**, 879–898 (2011).
59. Babayevska, N. *et al.* ZnO size and shape effect on antibacterial activity and cytotoxicity profile. *Sci. Rep.* **12**, 8148 (2022).
60. Elliott, P., Ragusa, S. & Catchside, D. Growth of sulfate-reducing bacteria under acidic conditions in an upflow anaerobic bioreactor as a treatment system for acid mine drainage. *Water Res.* **32**, 3724–3730 (1998).
61. Küllerich, B., Van de Ven, W., Nielsen, A. H. & Vollertsen, J. Sulfide precipitation in wastewater at short timescales. *Water* **9**, 670 (2017).
62. Li, Y. *et al.* Bacterial distribution in SRB biofilm affects MIC pitting of carbon steel studied using FIB-SEM. *Corros. Sci.* **167**, 108512 (2020).
63. Jia, R., Yang, D., Xu, D. & Gu, T. Carbon steel biocorrosion at 80 C by a thermophilic sulfate reducing archaeon biofilm provides evidence for its utilization of elemental iron as electron donor through extracellular electron transfer. *Corros. Sci.* **145**, 47–54 (2018).
64. Jia, R., Yang, D., Al-Mahamedh, H. H. & Gu, T. Electrochemical testing of biocide enhancement by a mixture of D-amino acids for the prevention of a corrosive biofilm consortium on carbon steel. *Ind. Eng. Chem. Res.* **56**, 7640–7649 (2017).
65. Jia, R., Yang, D., Abd Rahman, H. B. & Gu, T. Laboratory testing of enhanced biocide mitigation of an oilfield biofilm and its microbiologically influenced corrosion of carbon steel in the presence of oilfield chemicals. *Int. Biodeterior. Biodegrad.* **125**, 116–124 (2017).

Author contributions

M.J. and M.B.E.H. wrote the manuscript. H.M, H.T. and M.B.E.H. edit the manuscript. H.M, H.T. and M.B.E.H. supervised the project and revised the manuscript. All authors read and approved the final manuscript.

Funding

This research did not receive any specific grant from funding agencies in the public, commercial, or not-for-profit sectors.

Competing interests

The authors declare no competing interests.

Additional information

Supplementary Information The online version contains supplementary material available at <https://doi.org/10.1038/s41598-024-70654-6>.

Correspondence and requests for materials should be addressed to H.M. or M.-B.E.-H.

Reprints and permissions information is available at www.nature.com/reprints.

Publisher's note Springer Nature remains neutral with regard to jurisdictional claims in published maps and institutional affiliations.

Open Access This article is licensed under a Creative Commons Attribution-NonCommercial-NoDerivatives 4.0 International License, which permits any non-commercial use, sharing, distribution and reproduction in any medium or format, as long as you give appropriate credit to the original author(s) and the source, provide a link to the Creative Commons licence, and indicate if you modified the licensed material. You do not have permission under this licence to share adapted material derived from this article or parts of it. The images or other third party material in this article are included in the article's Creative Commons licence, unless indicated otherwise in a credit line to the material. If material is not included in the article's Creative Commons licence and your intended use is not permitted by statutory regulation or exceeds the permitted use, you will need to obtain permission directly from the copyright holder. To view a copy of this licence, visit <http://creativecommons.org/licenses/by-nc-nd/4.0/>.

© The Author(s) 2024